# An Accurate Calibrate-Able Multiharmonic Active Load–Pull System Based on the Envelope Load–Pull Concept

Mohammad S. Hashmi, *Member, IEEE*, Alan L. Clarke, *Student Member, IEEE*, Simon P. Woodington, *Student Member, IEEE*, Jonathan Lees, Johannes Benedikt, and Paul J. Tasker, *Senior Member, IEEE*

***Abstract*—After calibration, since the systematic imperfections of the envelop load–pull (ELP) components were now fully accounted for, the user is able to rapidly set accurate terminations with full Smith chart coverage. This functionality has been achieved by optimizing the hardware configuration of the envelop load–pull concept. Development of a system whose systematic errors could be described by a magnitude invariant error flow model was critical. As a consequence, a robust calibration mechanism, that is analogous to the one-port error correction of a vector network analyzer, was exploited and comprehensively verified. After calibration, since the systematic imperfections of the ELP components were now fully accounted for, the user is able to set accurately terminations with full Smith chart coverage.**

**Finally, measurements on commercially available transistor devices are presented that verify the rapid nature, accuracy, flexibility, reliability, and ease of calibration of the multiharmonic load–pull system.**

***Index Terms*—Active closed-loop load–pull, harmonic load–pull, nonlinear measurements, rapid load–pull calibration.**

## I. Introduction

LOAD–PULL is a key tool employed in large-signal device characterization, measurement, and design at microwave frequencies, necessary for the synthesis of a variable load impedance environment [1]–[4]. One important application of load–pull is in developing device modeling strategies [5], [6]. In order to develop accurate computer-aided design (CAD)-based models, devices must be characterized under many different large-signal operation conditions. Hence, there is a need for rapid highly accurate load–pull measurement systems to support CAD-based design.

Traditional load–pull systems are grouped into two categories, namely passive load–pull [7] and active load–pull [8], [9]. Passive load–pull involves a direct characteristic impedance transformation, generally realized through stub tuners. The major drawback of these passive systems is their inability to overcome inherent measurement system losses and thereby provide only a limited Smith chart coverage and load reflection coefficient range. Alternatively, active systems [8] can be used to overcome these losses by injecting amplified signal into the device output port, thus providing full coverage of the Smith chart.

Active systems can be realized using open- or closed-loop approaches. Open-loop active systems [8], although unconditionally stable, can be prohibitively slow due to the iterative and convergent nature of load setting. The closed-loop active load–pull system, reported in [9], overcomes this problem, but suffers from an inherent stability problem that can be mitigated by introducing highly selective RF bandpass filters in the loop [10]. Another alternative approach for achieving closed-loop load–pull has been reported in [11] and [12] and is called envelope load–pull (ELP). This system achieves stability by default due to the bandpass filter characteristics of the control unit employed in the design of the system. Thus, ELP is a logical active replacement for passive load–pull.

Consider first the logical development of passive load–pull. A passive load–pull system based on a simple manually controlled mechanical tuner is not reproducible, therefore cannot be pre-calibrated and must ideally be measured *in situ*. There have been significant efforts and investments from companies such as Maury Microwave, Ontario, CA, and Focus Microwave, Montreal, QC, Canada, to make the passive system repeatable, accurate, and reliable. As a consequence, these passive load–pull systems can now be robustly pre-calibrated. However, it must be noted that the pre-calibration of the tuners used in the passive load–pull systems can be very tedious and time consuming [13]. This slow pre-calibration of the tuners also lowers the overall measurement throughput [13]. However, while active closed-loop systems have also undergone several improvement and development cycles demonstrating excellent performance [2], there is no published report of a pre-calibrated closed-loop system.

It was thus imperative that the alternate closed-loop active ELP also underwent similar developmental changes with the objective of achieving accurate and repeatable performance that could support pre-calibration. This required further development of the ELP concept to significantly improve its repeatability and accuracy. It was reported in [11] that the nonideal operation of the system can be represented by an error flow model.

Manuscript received August 05, 2009. First published February 08, 2010; current version published March 12, 2010. This work was supported in part by the Engineering and Physical Research Council (EPSRC), Automatic Radio Frequency Techniques Group (ARFTG), Mimix Broadband (Europe), and Cobham, and in part by the ARFTG under a fellowship.

M. S. Hashmi was with the Centre for High Frequency Engineering, Cardiff University, Wales CF24 3AA, U.K. He is now with the iRadio Lab, University of Calgary, Calgary, AB, Canada T2N 1N4 (e-mail: mshashmi@ucalgary.ca).

A. L. Clarke, S. P. Woodington, J. Lees, J. Benedikt, and P. J. Tasker are with the Centre for High Frequency Engineering, Cardiff University, Wales CF24 3AA, U.K. (e-mail: Tasker@cf.ac.uk).

Color versions of one or more of the figures in this paper are available online at http://ieeexplore.ieee.org.

Digital Object Identifier 10.1109/TMTT.2010.2040403

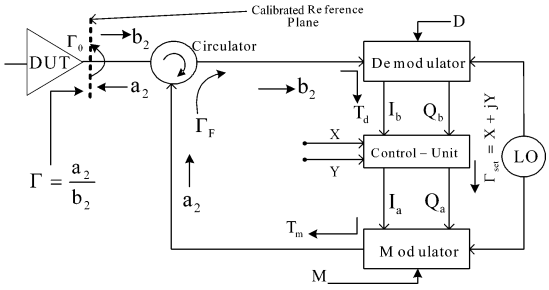


Fig. 1. Block diagram of ELP displaying the identified sources of errors in the loop components.

This model provides some key insight in helping advance the ELP development. The initial work in [12] is developed and furthered in this paper in a theoretical and practical manner, leading to a matured solution where it is possible to accurately and reliably pre-calibrate the developed active system. In addition, fewer measurements are required in the calibration of ELP compared to that of passive load–pull; hence, being very rapid with the potential to improve the measurement throughput.

## II. System Description and Error Flow Model Formulation

A generic block diagram of the ELP system is depicted in Fig. 1. For a detailed discussion on its theory of operation, the reader is referred to [11]. The signals $I_b$ and $Q_b$ are the baseband components of $b_2$, while $I_a$ and $Q_a$ are the baseband components of $a_2$. The required load reflection coefficient, assuming an ideal system, is simply given by setting the correct $X$ and $Y$ values in the "control unit," shown as follows in (1):

$$\Gamma_{\text{set}} = \Gamma = \frac{a_2}{b_2} \tag{1}$$

where

$$\Gamma_{\text{set}} = X + jY. \tag{2}$$

Ideally the load $\Gamma_{\text{set}} = X + jY$ presented by the ELP system should be the same as the load measured by the measurement. In practice, however, this is complicated by a number of factors limiting the accuracy of the system. These factors include systematic errors due to the nonideal nature of the demodulator, modulator, imperfect circulator directivity, delays, and losses in the cables, as displayed in Fig. 1.

To analyze and account for the systematic errors, an error flow model can be utilized, as reported in [11]. The ELP error model shown in Fig. 2 is an improved version of that reported in [11] with an additional term $\Gamma_F$ accounting for the effect of feedback and system isolation. The term $T_D$ refers to the demodulator conversion gain, as well as the external cabling and delays associated with the physical setup, whereas $D$ refers to the error contribution due to the dc offset generated in the demodulator. $\Gamma_{\text{set}} = X + jY$ refers to the required load reflection coefficient established by the external control variables $X$ and $Y$. $M$ is the contribution from the dc offset of the modulator, $T_M$ refers to the modulator conversion gain, as well as external cabling and delays, and $\Gamma_0$ is the passive impedance of the network. The error model reported in [11] ignored the effect of the factor $\Gamma_F$,

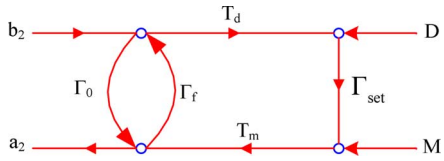


Fig. 2. Detailed "error flow model" of ELP system.

although it will be shown later in this paper that this factor plays an important role in realizing a pre-calibrate-able system.

The error flow model depicted in Fig. 2 can, by flow diagram analysis, lead to the following equation:

$$a_2 = \left(b_2 + \frac{1}{T_D}\left(D + \frac{M}{\Gamma_{\text{set}}}\right)\right) \times \left(\frac{\Gamma_{\text{set}} T_D T_M}{1 - \Gamma_F(\Gamma_{\text{set}} T_D T_M)} + \Gamma_0\right). \tag{3}$$

Since this equation cannot be rearranged to produce an explicated formulation of the measured load in terms of the set load $(X + jY)$, it is not possible to provide for a simple pre-calibration procedure. It is evident that the terms $D$ and $M$ in (3) are the problem. Therefore, as a first step to making the system simply pre-calibrate-able, it is important that these terms are eliminated. The approach presented in [11] adopted some dc offset pruning techniques, using external electronic circuitry, to nullify the effect of $D$ and $M$. These efforts were only partially successful. The reliability of this approach was severely limited [14] due to fact that the $D$ and $M$ terms turned out to be bias and drive dependent. Note the presence of $D$ and $M$ can be attributed to the fact that the ELP system reported in [11] and [14] was operated in the homodyne mode in order to maximize the bandwidth efficiency of the demodulator employed in the system.

It was thus concluded that the only practical way to eliminate the error terms $D$ and $M$ was to switch from the homodyne mode of operation used in [11] to a heterodyne mode of operation. With the RF information now being contained in the down-converted baseband sinusoid signals, high-pass filters can be placed at both the input and output of the "control-unit" to block the dc $D$ and $M$ terms, while allowing the sinusoid $I$ and $Q$ signals to propagate. The heterodyne mode of operation with the incorporation of high-pass filters allow for a simplification of the error flow model; hence, simplification of the system equation, in (3), to

$$\frac{a_2}{b_2} = \left(\frac{\Gamma_{\text{set}} T_D T_M}{1 - \Gamma_F(\Gamma_{\text{set}} T_D T_M)} + \Gamma_0\right). \tag{4}$$

Thus, the system can now be described by an explicit first-order control equation in (4). This equation describes the physical behavior of the ELP system and can be utilized to design a rapid, accurate, and reliable calibration mechanism for the system, as explained in Section III.

## III. Calibration of ELP System

It is important to understand the physical realization of the system before one looks into its calibration and application. The realization of the conceptual configuration presented in Fig. 1 is

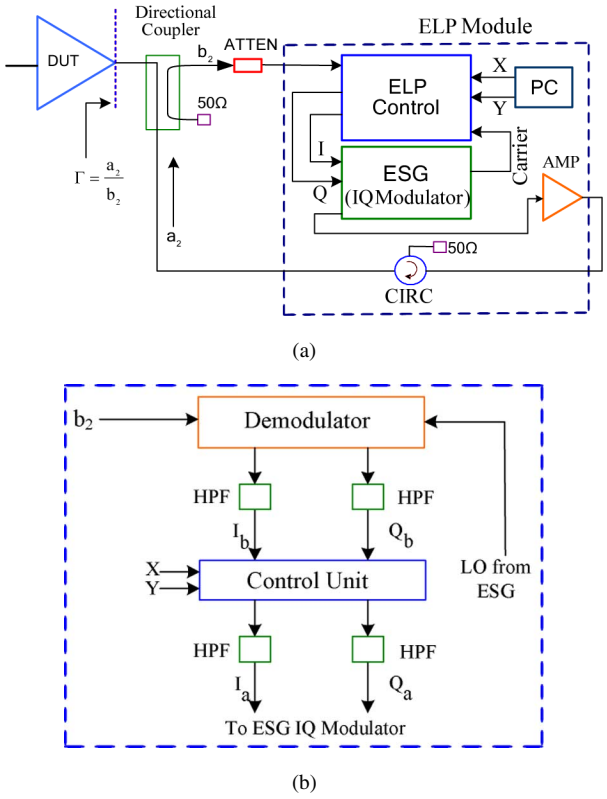


Fig. 3. (a) Block diagram of physically realized ELP loop. (b) Inner configuration of the "ELP Control" in (a).

displayed in Fig. 3(a). The directional coupler extracts the transmitted signal $b_2$, as well as isolating it from the injected signal $a_2$. The "ELP Control" comprises the demodulator, control unit, and the high-pass filters, as shown in Fig. 3(b). The demodulator used in this realization can operate over a frequency range of 0.8–2.7 GHz. External control variables, $X$ and $Y$, are supplied to the "ELP Control" from a computer-controlled DAC board. The up-conversion of the modified $I$ and $Q$ signals are carried out by the $Q$ modulator present in an Agilent vector signal generator (VSG).

The loop amplifier, shown in Fig. 3(a), compensates for any attenuation in the loop and ensures that the appropriate level of injected signal $a_2$ is maintained to achieve the requisite load reflection coefficient at the required reference plane. The realized load–pull system can be simply combined with any commercially available large-signal measurement system, such as an Agilent PNA-X, to achieve load–pull functionality. In the current investigation, the waveform engineering measurement system at Cardiff University, Wales, U.K. [15], based around the microwave transition analyzer (MTA) has been used to verify this system's performance.

The result in Fig. 4 displays the uncalibrated performance of the developed load–pull system. A spiral dataset of loads is chosen to provide full coverage of the Smith chart.

It can be clearly seen that, due to system imperfections, the measured loads do not match up with those set by the user of

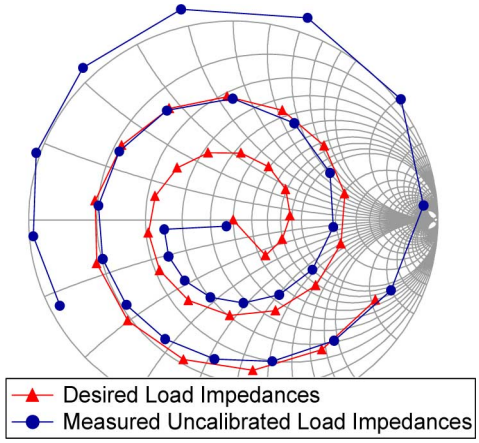


Fig. 4. Uncalibrated peformance of ELP over a 30-point set.

the system. Now the assumption is that this difference can be corrected by using the simplified error model given by (4). Since

$$\frac{a_2}{b_2} = \Gamma_{\text{meas}} \tag{5}$$

substituting (5) into (4) and rearranging gives

$$\Gamma_{\text{meas}} = \left( \frac{\Gamma_{\text{set}} \cdot G}{1 - \Gamma_F(\Gamma_{\text{set}} \cdot G)} + \Gamma_0 \right) \tag{6}$$

where $G$ represents the factor $T_D \times T_M$ and is termed the gain of the load–pull loop. It can be seen from (6) that if the load $\Gamma_{\text{set}}$ is set to zero, then the system's passive impedance $\Gamma_0$ term can be directly measured. By rearranging (6), we get (7) and (8), which are analogous to the one-port error model calibration equation used in any standard vector network analyzer (VNA) [16]

$$\Gamma_{\text{meas}} = \Gamma_0 + \Gamma_{\text{meas}} \cdot \Gamma_{\text{set}}(\Gamma_F \cdot G) + \Gamma_{\text{set}}[G(1 - \Gamma_0 \cdot \Gamma_F)] \tag{7}$$

$$\Gamma_{\text{meas}} = A + B \cdot \Gamma_{\text{meas}}\Gamma_{\text{set}} + C \cdot \Gamma_{\text{set}} \tag{8}$$

where $A = \Gamma_0, B = \Gamma_F. G$ and $C = G(1-\Gamma_0 \cdot \Gamma_F)$. To evaluate (8), only three distinct measurements need to be made for three different load settings to determine the unknown terms $A, B$, and $C$. This is one of the system's important novelties in that it can be calibrated quickly with very few different load measurements. Yet to improve the accuracy of the system and to minimize the error in the achieved result, due to measurement noise, it is advantageous to use a "least squares method" with multiple measurements with different load magnitudes and phases. After finding the terms $A, B$, and $C$, the values of the required error terms can be calculated by equations given in (9)–(11) as follows:

$$\Gamma_0 = A \tag{9}$$

$$G = C + BA \tag{10}$$

$$\Gamma_F = \frac{B}{G}. \tag{11}$$

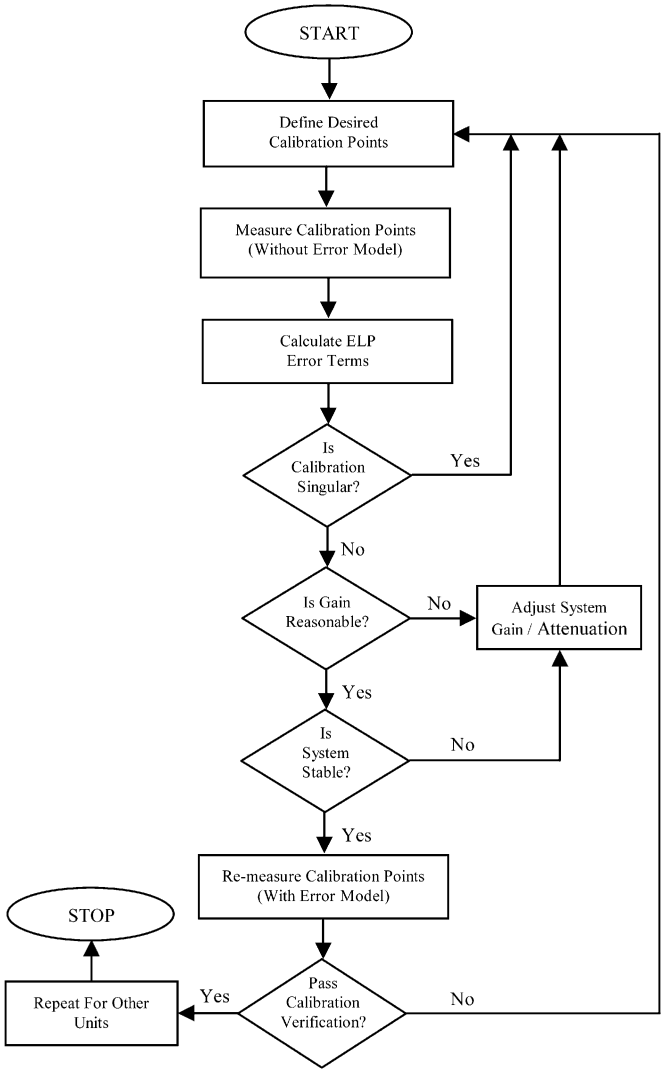


Fig. 5. Flowchart for solving the imperfections in the ELP system.

The flowchart shown in Fig. 5 describes the overall calibration procedure. A calibration data set is defined by sweeping the control variables $X$ and $Y$ around a spiral and the system is operated in the uncalibrated mode, attempting to acquire these loads. The error terms are then calculated and the system checks if the gain $G$ is realizable. If the check returns negative, then the attenuator or the loop amplifier setting, as shown in Fig. 3(a) and (b), is changed and the system is operated again until the check returns positive.

Upon the positive result on gain check, the system is assessed for stability by utilizing (12), which can be derived from (4) as follows:

$$1 > |\Gamma_F(\Gamma_{\text{set}} T_D T_M)|. \tag{12}$$

If the system fails the stability test then appropriate adjustments in the load–pull loop component setting, shown in Fig. 3(a) and (b), is carried out so that the system passes the stability check.

After obtaining the parameters in (8) through the process outlined in Fig. 5, the quantitative error flow model is determined

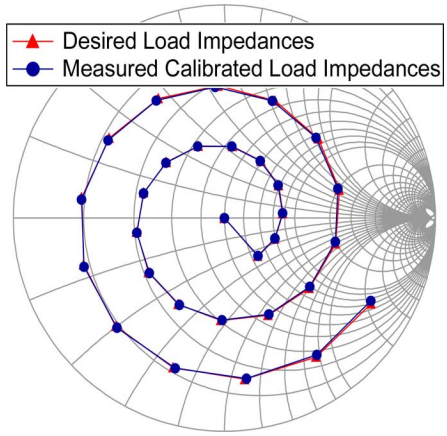


Fig. 6. Measured loads after incorporation of error model over a 30-point data set.

and can be applied to allow the user to correctly set the desired loads. To verify both the system functionality and validity of the error model, the calibrated system is now operated to correctly set the original desired load spiral. This is achieved by computing an alternative set of control settings $(X + jY)$ and employing (13) with the incorporation of the error coefficients

$$\Gamma_{\text{set}} = \frac{1}{G}\left(\frac{\Gamma_{\text{meas}} - \Gamma_0}{\Gamma_F(\Gamma_{\text{meas}} - \Gamma_0) + 1}\right). \tag{13}$$

The calibrated measured data points are displayed in Fig. 6. The achieved result is a clear proof that the imperfections in the loop components have been correctly accounted for by the improved error model. Thus, it can be concluded that this active closed-loop load–pull system can be quantified by an error model, analogous to the one-port error model of a VNA, which after calibration can be used to achieve repeatable and reliable user-defined impedance setting covering the entire Smith chart.

As previously stated, analogous with a VNA calibration, the ELP error model can be determined via the setting and measurement of three independent loads. However, this result in measurement errors associated with noise, producing flawed error coefficients. This error could be overcome by increasing the number of measurements. In the case of calibrating a VNA, this obviously requires more known standards, and thus, an increase in the number of new connections. In the case of ELP, neither applies since the load is set electronically. Hence, an increased number of measurements, set with ease, should allow for much improved error coefficient determination. The accuracy of the achieved results of the system can be quantified, in terms of percentage error $e$, using (14), where $N$ is the number of calibration points in the data set

$$e = \left(1/N \sum_{3}^{N} \frac{|\Gamma_{\text{meas}} - \Gamma_{\text{set}}|}{|\Gamma_{\text{set}}|}\right) \times 100. \tag{14}$$

It is clear from Table I, which records the percentage error against number of points used in the initial data set (the sprial), that the accuracy improves with the number of calibration points in the data set.

As a compromise between speed and accuracy, it is safe to assume that a calibration sequence utilizing 12–20 points will

TABLE I
AVERAGE DIFFERENCE BETWEEN DESIRED AND MEASURED IMPEDANCE VALUES AFTER CALIBRATION AND VERIFICATION

| *No. of Calibration Points, N* | *e (%)* | *No. of Calibration Points, N* | *e (%)* |
|---|---|---|---|
| 3 | 0.0456 | 12 | 0.0258 |
| 8 | 0.0337 | 20 | 0.0239 |
| 10 | 0.0271 | 30 | 0.0224 |

TABLE II
AVERAGE DIFFERENCE BETWEEN DESIRED AND MEASURED IMPEDANCE POINTS OVER 12 CALIBRATION DATA POINTS

| *Carrier Frequency (MHz)* | *e (%)* | *Carrier Frequency (MHz)* | *e (%)* |
|---|---|---|---|
| 850 | 0.0252 | 1800 | 0.0258 |
| 900 | 0.0255 | 2100 | 0.0259 |

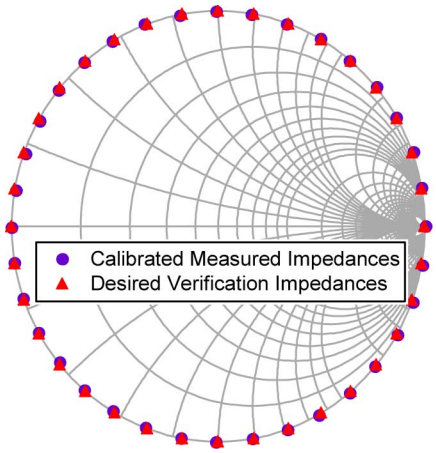


Fig. 7. Evaluation of the ELP calibration process over a 36-point data set.

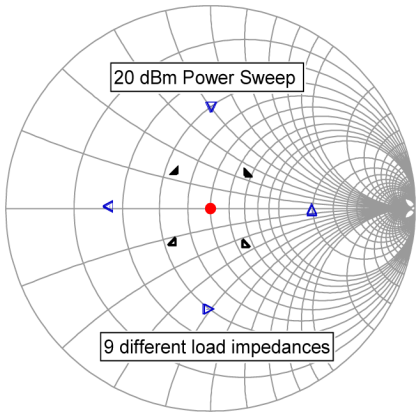


Fig. 8. Power sweep for a dynamic range of 20 dB showing the power-handling capability of the ELP system.

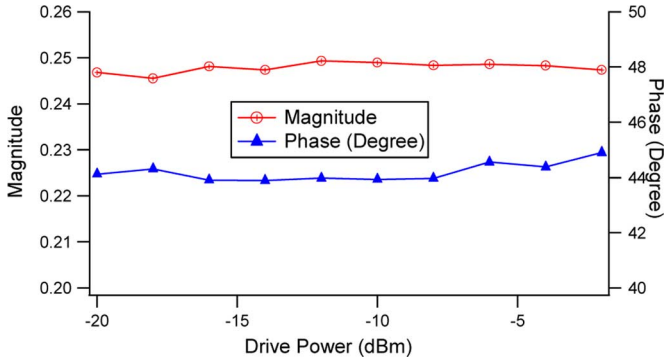


Fig. 9. Power sweep over a dynamic range of 20 dB for the load impedance of $0.25\angle 45°$.

provide a suitably accurate and reliable result. It is also important to note that the calibration accuracy is independent of carrier frequency, as shown in Table II. The only criterion for the selection of carrier frequency is that it should fall within the operating range of the demodulator and modulator used in the design of the system.

## IV. PERFORMANCE EVALUATION OF THE SYSTEM

Further evaluation of the calibration performance is extremely important for testing its accuracy. For the purpose of evaluation, a desired data set is defined at the extreme edge of the Smith chart at every ten degrees, i.e., 36 points. The calibrated load–pull system is then operated and the actual required load is measured. The obtained result is given in Fig. 7. In the current evaluation over 36 points, the achieved loads after the calibration are within 0.021% of the desired loads. Thus, it can be concluded that the developed calibration mechanism is accurate and reliable.

For the case under investigation, the calibration over a 30-point data set takes 15 min and the evaluation over 36 points takes another 18 min. Thus, on an average, the developed load–pull can be calibrated and employed in measurement applications in just over 30 min, unlike the passive tuner, which typically needs pre-characterization over hundreds of points, covering all the frequency ranges, which requires significantly more time [13]. Thus, the developed design and calibration strategy of ELP provides the opportunity for significantly improved measurement throughput.

One of the most important aspects of any load–pull system is its power-handling capability, as in many applications power sweep characterizations are often used for nonlinear transistor model validations. To demonstrate the power-handling capability of the developed load–pull system, the fundamental impedance was swept over a 20-dB dynamic range for nine different load settings, while keeping the second and third harmonic impedances actively matched to 50 Ω. Fig. 8 shows a power sweep result for nine different load impedances, respectively, while Fig. 9 presents the magnitude and phase of one load impedance swept over a dynamic range of 20 dB. The loads exhibit a variation of less than 0.5% in magnitude and less than 1.1° in phase for the dynamic range of 20 dB.

The results in Figs. 8 and 9 clearly demonstrate that the load emulation is independent of drive level. However, it is important to note that the dynamic range of the developed load–pull system is dependent on the linear operating range of the demodulator, modulator, and loop amplifier. In the current development, the loop amplifier is driven at 10-dB backed-off condition to operate in the linear domain. The ELP system can operate well for DUTs up to 4 W, and thus, is apt for characterization of on-wafer devices.

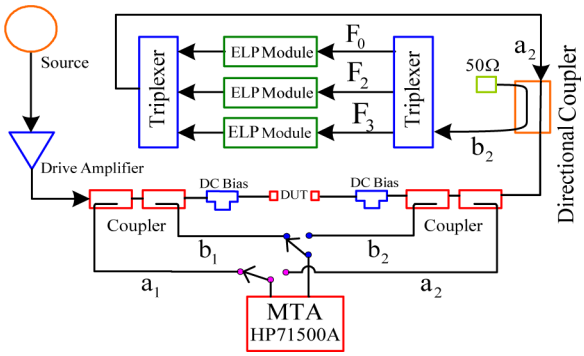


Fig. 10. Configuration of the multiharmonic ELP system within the MTA-based Cardiff University time-domain measurement system.

TABLE III
AVERAGE DIFFERENCE BETWEEN DESIRED AND MEASURED IMPEDANCE VALUES FOR EACH HARMONIC AFTER CALIBRATION AND VERIFICATION

| *No. of Calibration Points* | *Fundamental ($F_0$)* | *Second Harmonic ($F_2$)* | *Third Harmonic ($F_3$)* |
|---|---|---|---|
| 12 | 0.0252 | 0.0258 | 0.0276 |
| 20 | 0.0237 | 0.0243 | 0.0259 |

The current development could find it difficult to load–pull DUTs of the order of 10 W and above. However, appropriate changes could be incorporated to employ ELP in the load–pulling of higher power devices. High-power impedance transformers could be utilized to lower the linear output power requirements from the loop amplifier [18]. Another alternative could be to use the developed system in a hybrid setup with a passive load tuner such as used in [19].

Overall it has been proven that the system, when appropriately configured and operated, is drive-level independent and can be calibrated accurately in a rapid manner. This has the potential to improve the measurement throughput significantly as compared to active open-loop load–pull, which is extremely slow [4], and passive load–pull, which requires time-consuming pre-characterization of the tuners [13].

## V. EXTENSION OF SYSTEM TO MULTIHARMONIC DOMAIN

The reliable design and robust calibration of the ELP system allows a straightforward extension to a multiharmonic realization, as shown in Fig. 10. For multiharmonic system evaluation, a 1-W GaAs field-effect transistor (FET) was employed being driven into compression in such a way that the second and third harmonic powers are significant. The carrier frequency was chosen as 850 MHz.

The first step in utilizing this setup is to calibrate each of the ELP modules. Table III presents the outcome of the calibration verification for each of the modules. It can be seen in Table III that the accuracy of calibration is independent of the harmonic power and supports the results presented in Table II. There is a very slight difference in the accuracy at different harmonics, but it will be shown that this does not affect the measurement results.

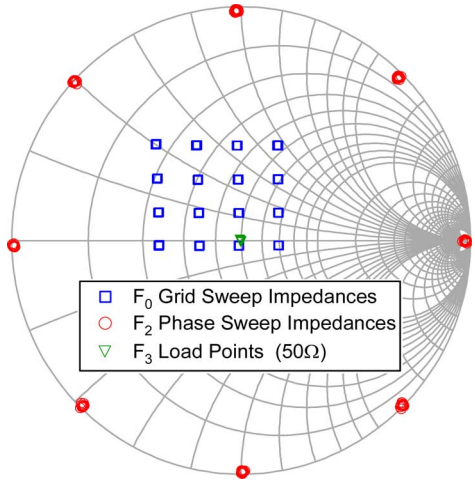


Fig. 11. Measurement showing the independent harmonic load setting capability of the developed ELP system.

TABLE IV
FUNDAMENTAL AND SECOND HARMONIC LOAD IMPEDANCE VALUES FOR DISCOVERING CONTOURS OF HIGH DRAIN EFFICIENCY AND OUTPUT POWER

| *Re{$Z_0$}* | *Im{$Z_0$}* | *Re{$Z_2$}* | *Im{$Z_2$}* |
|---|---|---|---|
| 94 | 116.9 | 0 | -104.1 |
| 95 | 93 | 0 | -82.2 |
| 99 | 70.5 | 0 | -61.6 |
| 100 | 48 | 0 | -38.8 |
| 100 | 27.7 | 0 | -16.9 |
| 100 | 8.8 | 0 | 3.9 |
| 100 | -10.5 | 0 | 25.2 |
| 100 | -26.6 | 0 | 44.5 |
| 100 | -42 | 0 | 60.7 |
| 100 | -58.1 | 0 | 81 |
| 100 | -61.9 | 0 | 88.1 |
| 100 | -70.2 | 0 | 95.6 |
| 100 | -78.2 | 0 | 103.8 |
| 100 | -86.1 | 0 | 110.2 |
| 100 | -93.7 | 0 | 117.3 |

It can be inferred from Tables II and III that the developed calibration mechanism is independent of the frequency of operation and the power level of the $a_2$ and $b_2$ traveling waves.

Another extremely important property of the developed system is its ability to set harmonic loads that are insensitive to each other [12]. To demonstrate this property, the fundamental impedance was swept over a $4 \times 4$ impedance grid, while for each fundamental, the phase of the second harmonic load was varied in 45° steps around the extreme edge of the Smith chart. The third harmonic was actively held at 50 Ω using the ELP module. It is evident from Fig. 11 that the harmonic impedances are uncoupled and unaffected by each other.

In this investigation, the whole sweep involved capturing only 128 measurements using the developed system, which on a similar open-loop harmonic load–pull system would require at least 15 times this (≈1920 measurements) due to the system needing to iterate and converge on the harmonic load impedances. This is an extremely important characteristic of the developed load–pull system, proving very useful, for example,

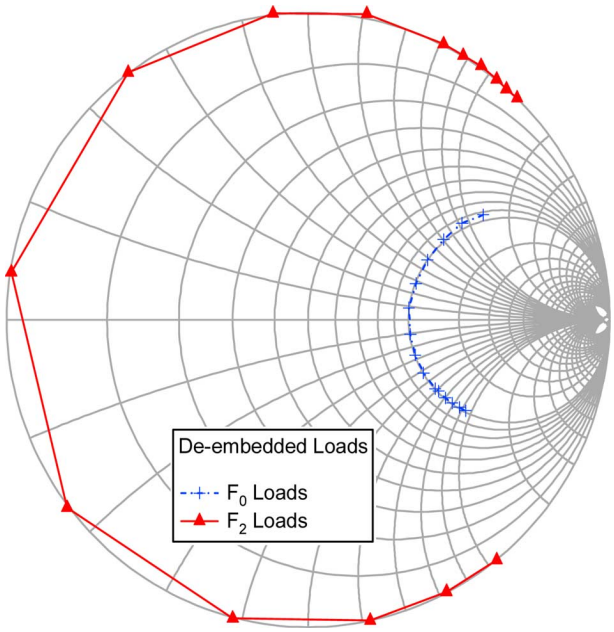


Fig. 12. Robust harmonic load impedance control by employing the developed harmonic ELP system.

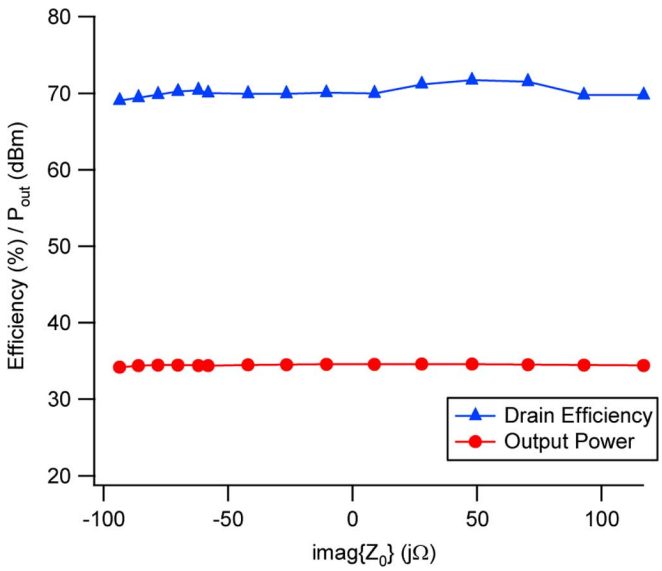


Fig. 13. Demonstration of constant power output and efficiency with respect to changing reactance through the use of ELP.

in reducing the required characterization time in the design of high-efficiency harmonically tuned PAs.

The independent harmonic load setting feature of the multiharmonic ELP system is now utilized in a specific investigation using a different device, a 2-W GaN pseudomorphic HEMT (pHEMT), where it was required to relate the fundamental and second harmonic impedances presented to the device in a specific manner, as given in Table IV, in order to discover contours of continuous high drain efficiency and output power [20].

Fig. 12 displays the resultant loads measured at the package plane for the 15 specific measurement points, where the fundamental and second harmonic impedances are tracking their real impedance contours. The third harmonic is arbitrarily terminated. It is evident that the measured harmonic loads are exactly as specified in Table IV. This demonstration proves that the calibration of the ELP modules was suitably reliable and robust in order to set harmonic loads independently, as required without the need of further iterations to converge on the correct impedances.

Fig. 13 displays the output power and efficiency measurements under these loading conditions, showing that the contour of constant efficiency and output power was located, with a less than one percentage point deviation in drain efficiency around 70% and only 0.1-dB variation in the 34.5-dBm output power over the range—the result that was expected. This investigation has demonstrated the necessity and value of the ELP calibration in establishing the desired impedances. It is also important to note that it would be extremely slow to conduct such an investigation using the active open-loop technique and probably impossible on passive load–pull systems.

## VI. Summary and Conclusion

This paper has presented an accurate pre-calibrate-able multiharmonic closed loop active load–pull system that is based on the envelope baseband-feedback load–pull concept. It was shown that a critical requirement for this to be achieved is that the ELP hardware implementation had to be modified so that it could be described by an explicit first-order control equation. These hardware modifications involved switching from homodyne to a heterodyne mode of operation. This allowed for the incorporation of high-pass filters into the system to eliminate the systematic error terms preventing an explicit error model formulation. As a consequence, an error flow model, which is analogous to the one-port error model of a VNA, can be defined to account for the systematic errors of the load–pull system. The inclusion of the feedback term in the error model is important for the system's accuracy and repeatability.

Robust calibration of the developed system was achieved by performing a set of measurements on a locus of impedances defined by a spiral. A spiral was chosen since it provides excellent coverage of the Smith chart both in terms of magnitude and phase. The accuracy of the load setting functionality after calibration is, due to measurement noise, slightly dependent on the number of points in the measured calibration data set. However, since these measurements are fully computer controlled and the load points are set electronically, increasing the number of measurement points, apart from speed, provide for no additional measurement disadvantages. The experimental investigation proves that the accuracy improvement is minimal beyond 20 points. The calibration methodology is independent of the frequency of operation and the drive power. Through rigorous validation procedures the pre-calibrated ELP system has been shown to be accurate and repeatable in a variety of situations.

Hence, both in terms of its calibration and operation, these systems will provide for improved measurement throughput over existing passive load–pull systems. The reliable pre-calibration operation also allows the easy extension of the ELP concept into the harmonic domain. The unique characteristic of the multiharmonic system is its independent load setting at different harmonics.

## ACKNOWLEDGMENT

The authors would like to acknowledge Dr. T. Williams, Selex Galileo, Luton, U.K., for his valuable time and interesting discussions, and R. Pengelly, CREE, Durham, NC, for supplying the GaN device used.

## REFERENCES

[1] R. S. Tucker and P. D. Bradley, "Computer-aided error correction of large-signal load–pull measurements," *IEEE Trans. Microw. Theory Tech.*, vol. MTT-32, no. 3, pp. 296–300, Mar. 1984.

[2] F. Blache, J. M. Nebus, P. Bouysse, and J. P. Villotte, "A novel computerized multiharmonic load–pull system for the optimization of high efficiency operating classes in power transistors," in *IEEE MTT-S Int. Microw. Symp. Dig.*, Jun. 1995, pp. 185–187.

[3] F. De Groote, O. Jardel, J. Verspecht, D. Barataud, J.-P. Teyssier, and R. Quere, "Time domain harmonic load–pull of an AlGaN/GaN HEMT," in *Proc. 66th ARFTG Conf.*, Washington, DC, Dec. 2005, pp. 142–145.

[4] J. Benedikt, R. Gaddi, P. J. Tasker, and M. Goss, "High-power time-domain measurement system with active harmonic load–pull for high-efficiency base-station amplifier design," *IEEE Trans. Microw. Theory Tech.*, vol. 48, no. 12, pp. 2617–2624, Dec. 2000.

[5] H. Qi, J. Benedikt, and P. Tasker, "Novel nonlinear model for rapid waveform-based extraction enabling accurate high power PA design," in *IEEE MTT-S Int. Microw. Symp. Dig.*, Jun. 2007, pp. 2019–2022.

[6] S. Woodington, T. Williams, H. Qi, D. Williams, L. Pattison, A. Patterson, J. Lees, J. Benedikt, and P. J. Tasker, "A novel measurement based method enabling rapid extraction of a RF waveform look-up table based behavioral model," in *IEEE MTT-S Int. Microw. Symp. Dig.*, Jun. 2008, pp. 477–480.

[7] R. B. Stancliff and D. P. Poulin, "Harmonic load–pull," in *IEEE MTT-S Int. Microw. Symp. Dig.*, Jun. 1979, pp. 185–187.

[8] Y. Takayama, "A new load–pull characterization method for microwave power transistors," in *IEEE MTT-S Int. Microw. Symp. Dig.*, Jun. 1976, pp. 218–220.

[9] G. P. Bava, U. Pisani, and V. Pozzolo, "Active load technique for load–pull characterisation at microwave frequencies," *Electron. Lett.*, vol. 18, no. 4, pp. 178–180, Feb. 1982.

[10] A. Ferrero, V. Teppati, and U. Pisani, "Recent improvements in real-time load–pull systems," in *IEEE Instrum. Meas. Technol. Conf.*, Apr. 2006, pp. 448–451.

[11] T. Williams, J. Benedikt, and P. J. Tasker, "Experimental evaluation of an active envelope load–pull architecture for high speed device characterization," in *IEEE MTT-S Int. Microw. Symp. Dig.*, Jun. 2005, pp. 1509–1512.

[12] M. S. Hashmi, A. L. Clarke, S. Woodington, J. Lees, J. Benedikt, and P. J. Tasker, "Electronic multi-harmonic load–pull system for experimentally driven power amplifier design optimization," in *IEEE MTT-S Int. Microw. Symp. Dig.*, Jun. 2009, pp. 1549–1552.

[13] C. Roff, J. Graham, J. Sirois, and B. Noori, "A new technique for decreasing the characterization time of passive load–pull tuners to maximize the measurement throughput," in *Proc. 72nd ARFTG Conf.*, Dec. 2008, pp. 92–96.

[14] T. V. Williams, "A large signal multi-tone time-domain waveform measurement system with broadband active impedance control," Ph.D. dissertation, Dept. Elect. Electron. Eng., Cardiff Univ., Wales, U.K., 2007.

[15] D. J. Willimas and P. J. Tasker, "An automated active source and load–pull measurement system," in *Proc. 6th IEEE High-Freq. Postgrad. Colloq.*, Sep. 2001, pp. 7–12.

[16] D. M. Pozar, *Microwave Engineering*, 3rd ed. New York: Wiley, 2005.

[17] E. Kreyszig, *Advanced Engineering Mathematics*, 8th ed. New York: Wiley, 2000.

[18] Z. Aboush, J. Lees, J. Benedikt, and P. Tasker, "Active harmonic load–pull system for characterizing highly mismatched high power transistors," in *IEEE MTT-S Int. Microw. Symp. Dig.*, Jun. 2005, vol. 3, pp. 1311–1314.

[19] V. Teppati, A. Ferrero, and U. Pisani, "Recent advances in load–pull systems," *IEEE Trans. Instrum. Meas.*, vol. 57, no. 11, pp. 2640–2646, Nov. 2008.

[20] S. C. Cripps, P. J. Tasker, A. L. Clarke, J. Lees, and J. Benedikt, "On the continuity of high efficiency modes in linear RF power amplifiers," *IEEE Microw. Wireless Compon. Lett.*, vol. 19, no. 10, pp. 665–667, Oct. 2009.

**Mohammad S. Hashmi** (S'04–M'09) was born in India. He received the B.Tech. degree from Aligarh Muslim University, Aligarh, India in 2001, the M.S. degree from the Darmstadt University of Technology, Darmstadt, Germany in 2005, and the Ph.D. degree in nonlinear microwave instrumentation from Cardiff University, Wales, U.K., in 2009.

In Fall 2005, he joined Cardiff University. From March 2009 to July 2009, he held a postdoctoral position with Cardiff University. Since September 2009, he has been a Postdoctoral Fellow with the iRadio Lab, University of Calgary, Calgary, AB, Canada. He was with Philips Semiconductors, Nuremburg, Germany, and Thales Electronics, Berlin, Germany, during which time he was involved in the field of RF circuits and systems. His current research interest is the nonlinear characterization and linearization of power amplifiers for mobile and satellite applications and microwave instrumentation.

Dr. Hashmi was the recipient of the 2008 Automatic Radio Frequency Techniques Group (ARFTG) Microwave Measurement Fellowship.

**Alan L. Clarke** (S'08) received the M.Eng. degree in electronic engineering from Cardiff University, Wales, U.K., in 2007, and is currently working toward the Ph.D. degree in electronic engineering at Cardiff University.

He is currently with the Centre for High Frequency Engineering, Cardiff University. His research interests include the development of rapid active load–pull techniques and microwave device characterization for the power amplifier (PA) design process.

**Simon P. Woodington** (S'08) received the B.Eng. degree in electronic engineering from Cardiff University, Cardiff, U.K., in 2006, and is currently working toward the Ph.D. degree in electronic engineering at Cardiff University.

He is currently with the Centre for High Frequency Engineering, Cardiff University. His research interests include microwave device characterization and evolving microwave measurement systems.

**Jonathan Lees** received the M.Sc. and Ph.D. degrees from Cardiff University, Wales, U.K., in 2002 and 2006, respectively.

He is currently a Senior Research Associate with the Centre for High Frequency Engineering, Cardiff University, where his key research areas are linear-efficient power amplifier (PA) design, the characterization, design, and optimization of Doherty PAs, and the study of device nonlinearity and linearization using time- and envelope-domain techniques. His work in this area culminated in the first published GaN Doherty amplifier, and his more recent activities consider the development of novel high-power broadband time-domain measurement and load–pull techniques that directly address the current and future needs of modern communication systems. In June 2009, he assumed an additional role as a Senior Design Engineer supporting Mesuro Ltd., leading the commercial introduction of new measurement solutions that enable systematic waveform engineering at RF and microwave frequencies.

Dr. Lee has been a Chartered Engineer in the U.K. since 1999.

**Johannes Benedikt** received the Dipl.-Ing. degree in electrical engineering from the University of Ulm, Ulm, Germany in 1997, and the Ph.D. degree from Cardiff University, Wales, U.K., in 2002.

During this time, he took on an additional position as a Senior Research Associate with Cardiff University, starting in October 2000 supervising a research program with Nokia on RF power amplifiers (PAs). In December 2003, he became a Lecturer with Cardiff University with responsibility for furthering research in the high-frequency area. His main research focus is on the development of systems for the measurement and engineering of RF current and voltage waveforms and their application in complex PA designs. Since April 2009, he has undertaken the additional role of CTO at Mesuro Ltd., leading the commercial introduction of new measurement solutions that enable systematic waveform engineering at RF and microwave frequencies.

**Paul J. Tasker** (M'88–SM'08) received the B.Sc. degree in physics and electronics and Ph.D. degree in electronic engineering from Leeds University, Leeds, U.K., in 1979 and 1983, respectively.

From 1984 to 1990, he was a Research Associate with Cornell University, Ithaca, NY, where he was involved in the early development of HFET transistors. From 1990 to 1995, he was a Senior Researcher and Manager with the Fraunhofer Institute for Applied Solid State Physics (IAF), Freiburg, Germany, where he was responsible for the development of millimeter-wave monolithic microwave integrated circuits (MMICs). In Summer 1995, he joined the School of Engineering, Cardiff University, as Professor. While with Cardiff University, he has been establishing the Cardiff University and Agilent Technology Centre for High Frequency Engineering. The Centre's research objective is to pioneer the development and application of RF *I–V* Waveform and Engineering Systems, with a particular focus to addressing the PA design problem. He has contributed to over 200 journal and conference publications and given a number of invited conference workshop presentations.

Dr. Tasker is an IEEE Microwave Theory and Techniques Society (IEEE MTT-S) Distinguished Microwave Lecturer for 2008–2010.